Chapter 5

Design of a New Low Torque Ripple DSSRM

5.1 Introduction

In the previous chapters, it has been observed that DSSRM possess high torque ripple, especially in the commutation region. The high torque ripple is mainly the results of the salient pole structure and discrete excitation of phases. In the lower speed region, because of the low value of back EMF, the phase currents of SRMs and DSSRMs have the capability to reach the peak value. In this case, the phase currents are limited and shaped through the current chopping control method. The active torque ripple reduction techniques utilize the shaping of phase currents to reduce the torque ripple. The passive methods are also effective to reduce the torque ripple when current chopping mode is active. Therefore, these methods are mainly advantageous in lower speed region where current chopping control is active. Unlike this case, in the high-speed region, because of the high back EMF, the phase currents fail to reach the peak value and adopt the single-pulse control (SPC). In this case, the phases lose the possibility of shaping through the controller; therefore, these control techniques are generally not capable to significantly reduce the torque ripple in the higher speed operation.

In this chapter, the design methodology for a new low torque ripple DSSRM is proposed. The proposed motor has a significantly low torque ripple, especially in higher speed region when the phase currents reach to SPC mode or about to reach it. Taking the motivation from [93] that a DSSRM can be considered a combination of two SRMs, firstly,

a hypothetical machine has been suggested and investigated, in this work, which has a significantly low torque ripple. Thereafter, some design modifications are investigated in the proposed motor to acquire nearly same output response as in the hypothetical machine. The following points are notable in this regard:

1. DSSRM suffers from the high torque ripple problem and the level of torque ripple further increases in high-speed region.

2. Most of the active and passive torque ripple reduction techniques are applicable in current chopping control mode.

3. The proposed theory allows the designing of a new DSSRM which has a very low torque ripple when phase currents reach near single-pulse control mode.

The proposed theory would provide a possibility for future design and implementation of low torque ripple DSSRMs. The work presented here is basic and considers the theories of normal DSSRM for clear understanding.

5.2 Torque ripple in DSSRM in High Speed Region

In the high-speed region, the level of torque ripple in DSSRM is very high. In this chapter, the designing of a low torque ripple DSSRM is suggested and investigated, which has a significantly low torque ripple, especially in the high-speed region. Before going to the designing of the proposed motor, first, we should investigate the level of torque ripple in the case of normal DSSRM for its comparative analysis with the proposed motor. Fig. 5.1 shows the 2-D structure of a 3-phase radial flux 12/10 pole single-tooth winding DSSRM, which is considered as the normal or baseline DSSRM. The rotor shown is in its initial position, which is the unaligned condition with respect to phase A. Phase A coils are wound on the exciting poles $P_{A1}...P_{A4}$. The respective coils of phase B and phase C are wound on $P_{B1}...P_{B4}$ and $P_{C1}...P_{C4}$, respectively. Subtracting flux winding polarity is chosen to excite the consecutive phase windings. Fig. 5.2 represents half of its cross-section view, showing some of its linear and angular parameters. Table 5.1 enlists the specifications of the parameters of this motor. The rated speed, power and peak phase current considered are 1000 rpm, 3.5 kW and 30A, respectively. To increase

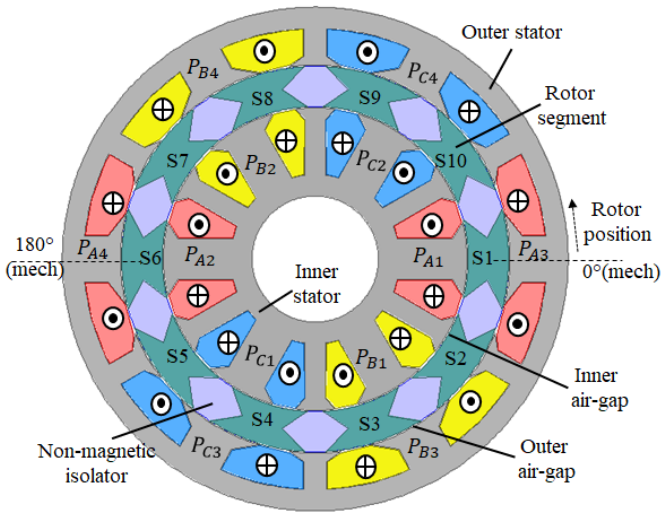

Figure 5.1: 2-D structure of a 3-phase radial flux 12/10 pole DSSRM.

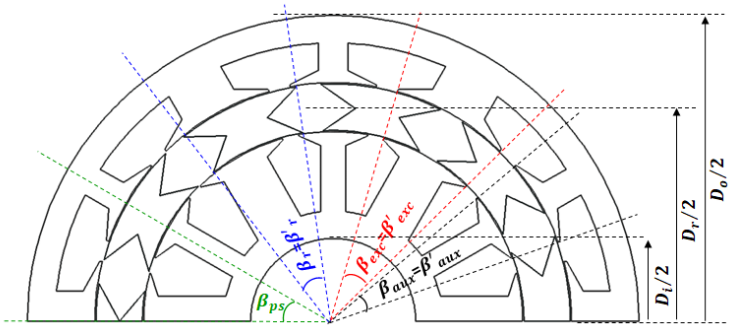

Figure 5.2: Representation of DSSRM design parameters.

the rated speed, the stator slot opening angle (β_{so}) is high in this case. To increase the rotor segments overlap area with exciting and auxiliary poles, for higher value of aligned inductance, β_r is considered higher than β_{exc} in this case. The value of β_{so} and stator/rotor arc angles are as listed in Table 5.1. This motor is preserved as DSSRM1 in this work.

The steady-state response of DSSRM1 is obtained through simulation study at the rated speed of 1000 rpm. Fig. 5.3 shows the steady-state waveforms of the phase currents and output torque. The peak phase current is 30 A. The phase turn-on and turn-off angles are 0°and 14.3° (mech.), respectively. Fig. 5.3 (a) shows that the phase currents are on the verge of the single-pulse control (SPC) mode. Fig. 5.3 (b) shows the variation of output torque with the rotor position at rated speed. The average torque (T_{avg}), peak-to-peak torque ripple (T_{pk2pk}) and % torque ripple (% T_{ripple}) are 33.6 N-m, 41.6 N-m, and 123.8%, respectively. This investigation shows the presence of a high torque ripple in this motor and divulges the need for further improvement in its torque pulsation behaviour.

Table 5.1: Design specifications of the baseline DSSRM.

Parameter	Value
Number of each stator poles/rotor segments	12/10
Outer and inner diameter of motor (D_o, D_i)	200 mm & 50 mm
Average diameter of rotor (D_r)	137 mm
Yoke height of inner and outer stator	8.5 mm
Axial length (l)	90 mm
Stator slot opening angle (β_{so})	9°
Inner and outer arc angle of rotor segments (β_r, β'_r)	30°
Arc angle of inner and outer stator exciting poles (β_{exc}, β'_{exc})	27°
Arc angle of inner and outer stator auxiliary poles (β_{aux}, β'_{aux})	15°
length of each air-gap (l_g)	0.5 mm
Number of conductors per slot (N_{slot})	54
Rated power (P_o)	3.5 kW
Rated Speed (N)	1000 rpm
Peak phase current	30 A
Stroke angle	12°

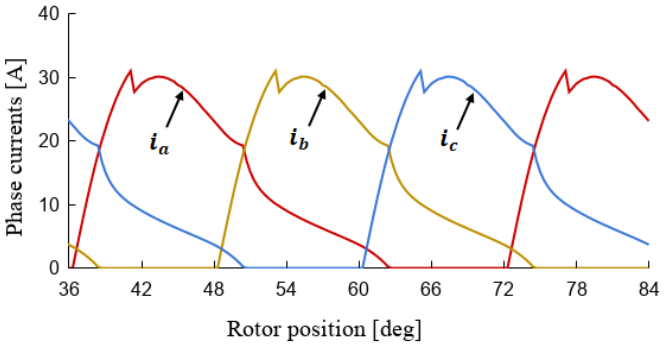

(a)

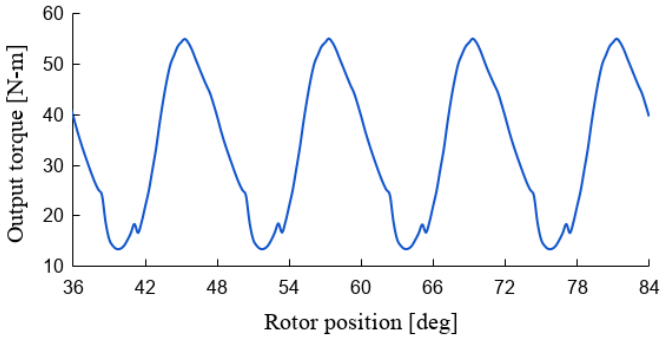

(b)

Figure 5.3: Simulated response of the DSSRM1 at rated speed of 1000 rpm. (a) Phase currents. (b) Output torque.

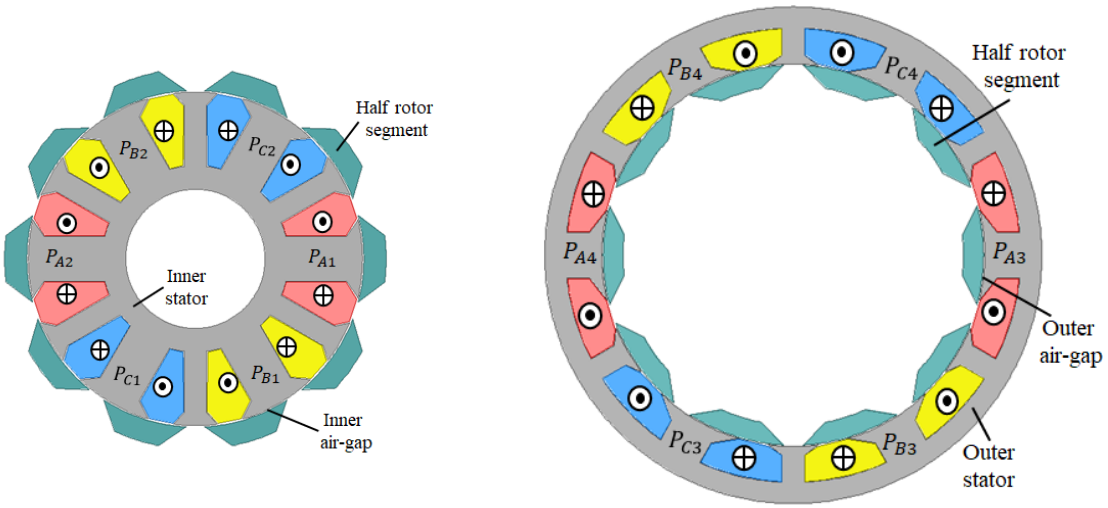

(a) (b)

Figure 5.4: Two separated parts of DSSRM1. (a) Inner SRM. (b) Outer SRM.

5.3 Design Hypothesis for a Low Torque Ripple DSSRM

A DSSRM can be considered a combination of two SRMs, inner SRM and outer SRM. Inner SRM consists of an inner stator, inner half part of the rotor, and inner stator coils. In the same way, outer SRM constitutes the outer stator, outer half part of the rotor, and outer stator coils. Fig. 5.4 shows these two SRMs, respectively. Fig. 5.5 shows the simulated dynamic response of these two SRMs in isolated condition at the rated speed with the peak phase current of 30 A. Figs. 5.5 (a) and 5.5 (b) show the waveforms of phase currents and torque with rotor position for the inner and outer SRM, respectively. It is seen in figures that the angular separation between two adjacent torque peaks is 12°, whereas the separation between a torque peak and the adjacent torque dip is nearly 6° in both machines. These values are equal to the stroke angle and half of the stroke angle, respectively. From this observation, it can be concluded that if both the SRMs are operated in isolated condition with the phase shift 6°; the rising torque region of one SRM will overlap with the falling torque region of the other one, resulting in a comparatively lower torque ripple profile.

To validate the above theory, a hypothetical DSSRM of the same dimensions as DSSRM1 is modelled, and its performance is simulated through FEM analysis. Fig. 5.6 shows the structure of the hypothetical DSSRM. The outer stator of this machine is shifted by half of the stroke angle i.e. 6° in the direction of rotation with respect to the

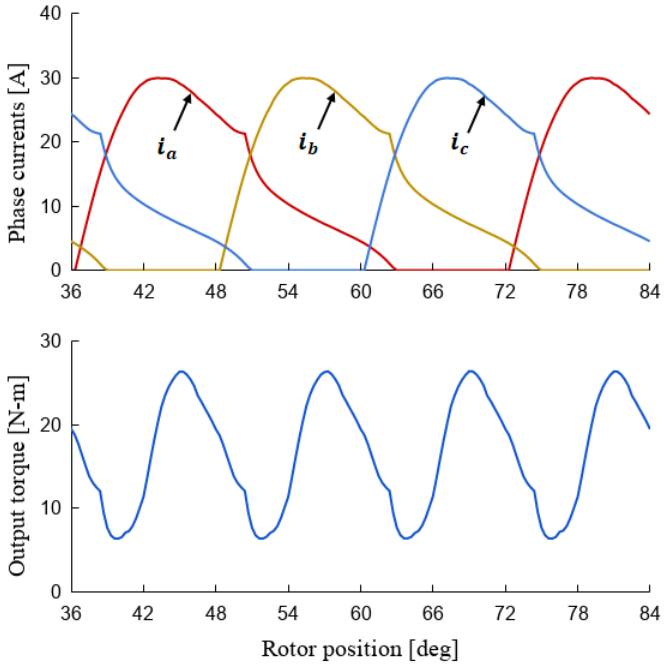

(a)

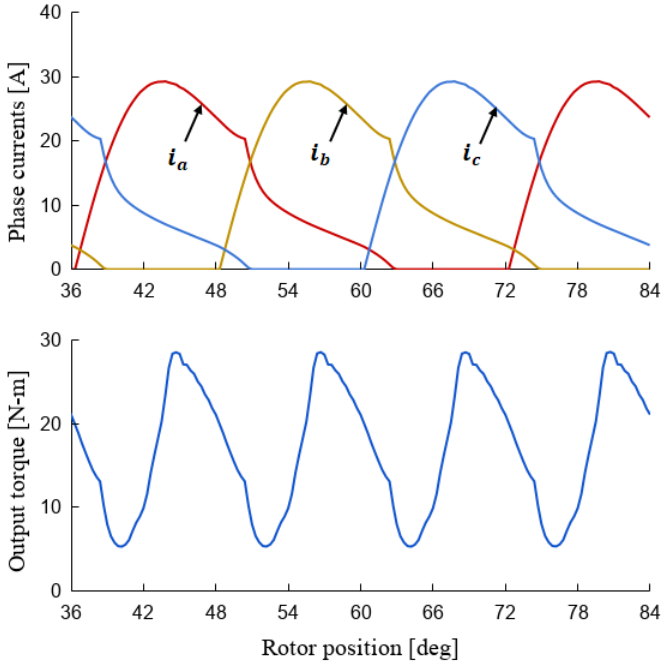

(b)

Figure 5.5: Steady-state response of two separated SRMs at rated speed. (a) Phase currents and torque of inner SRM. (b) Phase currents and torque of outer SRM.

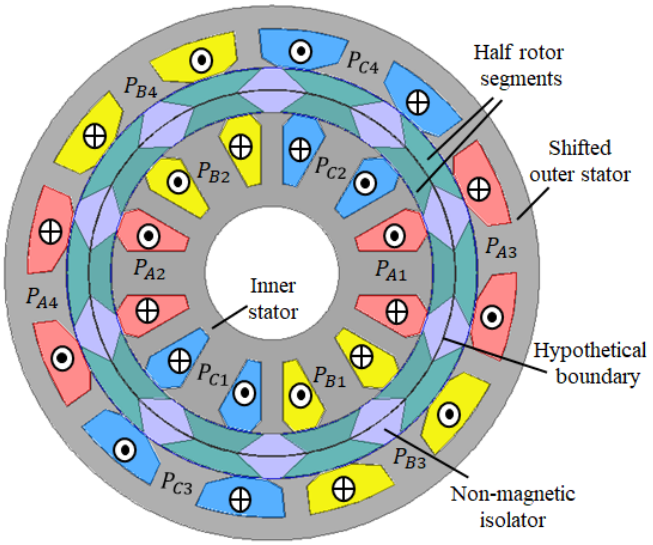

Figure 5.6: Structure of the hypothetical DSSRM2.

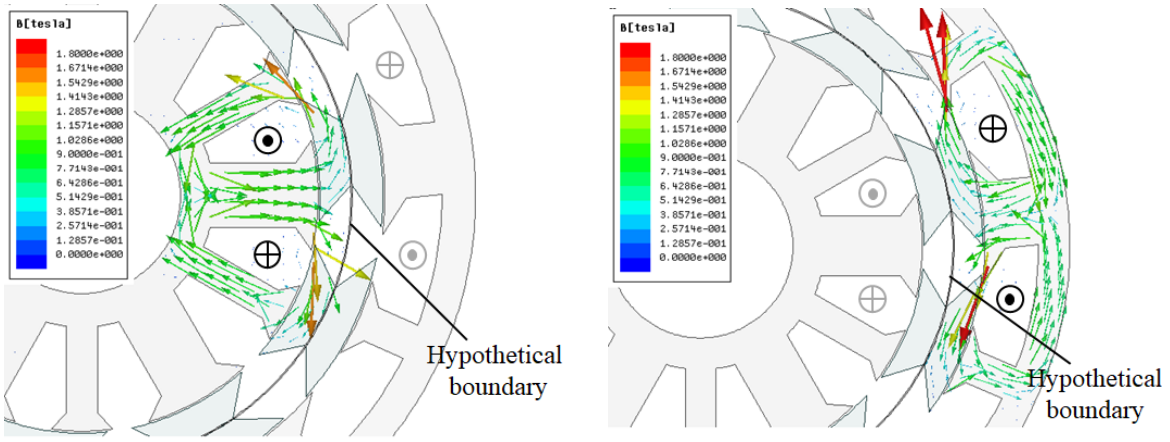

(a) (b)

Figure 5.7: Flux distribution in DSSRM2. (a) Flux distribution with the excitation of inner stator winding at 90° (elec.) rotor position. (b) Flux distribution with the excitation of outer stator winding at 150° (elec.) rotor position.

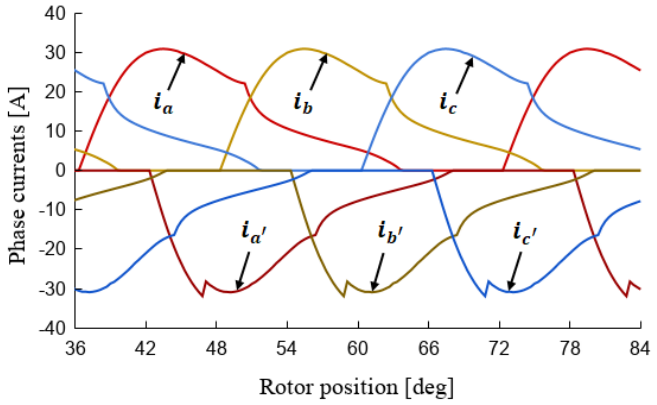

(a)

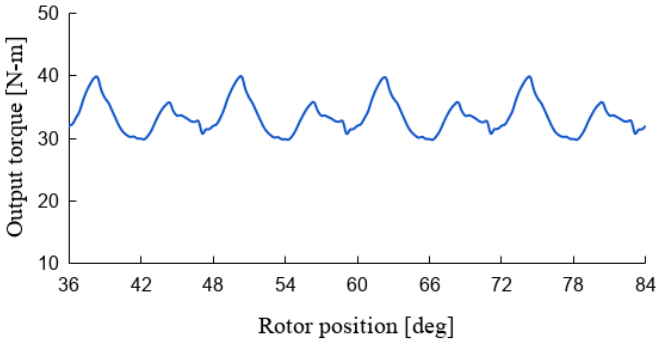

(b)

Figure 5.8: Simulated response of DSSRM2 at the rated speed. (a) Phase currents. (b) Dynamic torque.

inner stator. Each rotor segment is divided into two halves, called half rotor segments. A hypothetical boundary is injected between them. The hypothetical boundary diminishes all the normal component of the flux falling on its surface and provides the complete magnetic isolation between the inner and outer magnetic circuits. The phase windings of the outer stator are excited parallelly with a delay of 6° (mech.) with respect to the phase windings of inner stator. This hypothetical machine is renowned as DSSRM2 in this paper. The flux distribution in DSSRM2 is shown in Fig. 5.7 when the inner and outer stator phase windings are excited individually at 90° (elec.) and 150° (elec.) rotor positions, respectively, by 30 A. It is seen that because of the presence of the hypothetical boundary, the flux of the inner SRM does not link with the outer SRM and vice versa. In this way, the hypothetical boundary provides the complete magnetic isolation between the inner and outer magnetic circuits. Fig. 5.8 shows the simulated steady-state response of DSSRM2 at rated speed for the peak phase current of 30 A. In this figure, i_a, i_b, and i_c are the phase currents of the inner stator windings whereas $i_{a'}$, $i_{b'}$, and $i_{c'}$ are the phase currents of outer stator windings. The values of T_{avg}, T_{pk2pk}, and % T_{ripple} are 33.5 N-m, 10.2 N-m, and 30.4%, respectively, in this case. This investigation shows that torque ripple in DSSRM2 is inherently low as compared to DSSRM1. However, this machine is practically not implementable because such a hypothetical boundary is not possible in reality. For implementing a nearby machine in the real platform, some geometric modifications and compromises are suggested and investigated in this work. The design modifications for the proposed DSSRM containing the nearby response as in DSSRM2 are discussed in the next section.

5.4 Geometric Modifications in the Proposed DSSRM

As discussed in the previous section, the behaviour of the hypothetical boundary is to isolate the two magnetic circuits, i.e., inner and outer SRMs. However, during the implementation of the proposed DSSRM, considerable magnetic isolation can be provided between the two magnetic circuits by inserting a wider non-magnetic region between the half rotor segments. Due to the insertion of this region, although the inner SRM remains same, the dimensions of the outer SRM alter considerably. This results in the alteration of its magnetic behaviour. Therefore, to meet the nearby response as in DSSRM2,

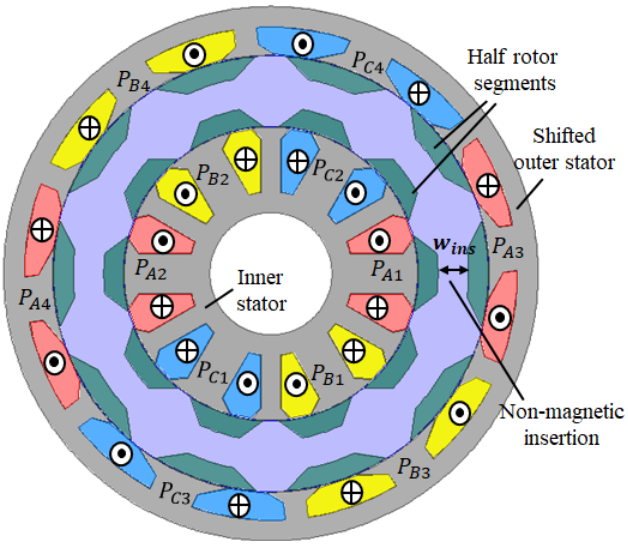

Figure 5.9: Initial structure of the proposed DSSRM.

some structural or geometric modifications are suggested and investigated in the proposed DSSRM. Fig. 5.9 shows the initial representation of the proposed DSSRM with the shifted outer stator and the half rotor segments with the insertion of a wider non-magnetic isolator of the width w_{ins} between them. The rotor segments can be assembled through a non-ferromagnetic cage, as suggested in [94]. This proposed machine will be further dealt with DSSRM3 in this work. The procedure for the modifications in the DSSRM3 is discussed in the further subsections.

5.4.1 Modification in the Pole Height of Outer Stator

With the insertion of the non-magnetic isolator between the half rotor segments, the slot area of the outer stator increases for the same pole height. However, the slot area should be kept same before and after the insertion because it carries the same number of conductors of the same cross-sectional area. To achieve the same slot area pole height of the outer stator should be reduced in the latter case. Fig. 5.10 (a) shows the inner radius (r), pole height (h_{pso}), and yoke height (h_{ys}) of outer stator before the insertion of the isolator. These values become ($r + w_{ins}$), h'_{pso}, and h_{ys}, respectively, after the insertion of the isolator of the width w_{ins}. The condition for the same slot area in both cases is as follows:

$$\pi\{(r + h_{pso}^2) - r^2\} - A = \pi\{(r + w_{ins} + h'_{pso})^2 - (r + w_{ins})^2\} - A' \tag{5.1}$$

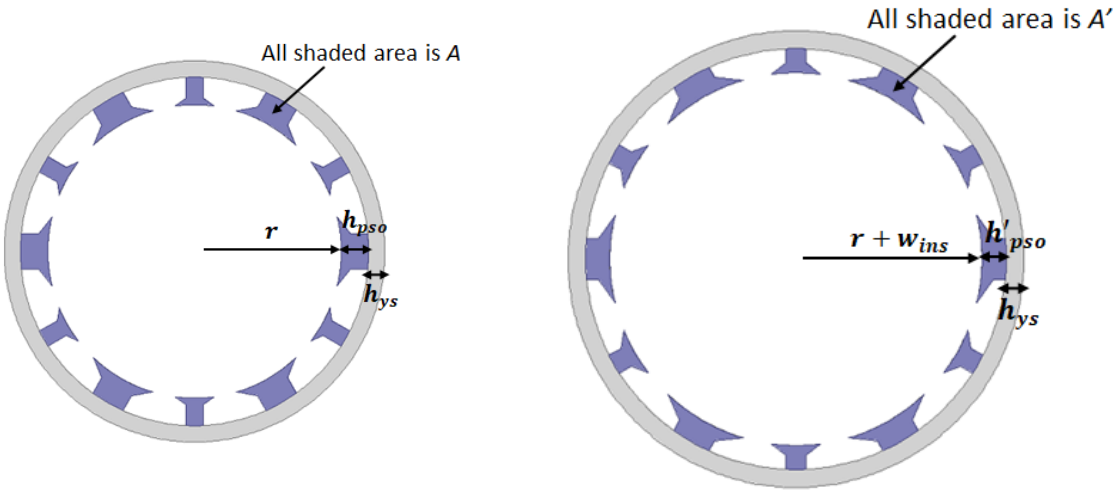

(a) (b)

Figure 5.10: Modification in the pole height (h_{pso}) of outer stator due to the insertion of the non-magnetic isolator of width w_{ins}. (a) Outer stator before insertion. (b) Outer stator after insertion ($h'_{pso} < h_{pso}$).

where A and A' are the cross-sectional areas covered by all the stator poles before and after the modification of the pole height of the outer stator. Fig. 5.10 clearly shows these areas with the shaded portion of the stator. Assuming that the same cross-sectional area is covered by the stator poles in both the cases (i.e., $A = A'$), the above condition is reduced to:

$$(r + h_{pso}^2) - r^2 = (r + w_{ins} + h'_{pso})^2 - (r + w_{ins})^2 \tag{5.2}$$

Eq. (5.2) can be used to calculate the approximate height of the outer stator poles h'_{pso} after the insertion of the non-magnetic isolator of the width w_{ins}. The exact height can be calculated through FEM analysis.

5.4.2 Calculation of the Width of the Non-Magnetic Region

The outer diameter of DSSRM3 increases with the insertion of the non-magnetic isolator between half rotor segments. There is a trade-off between the lower flux leakage between half rotor segments and smaller outer diameter of the motor. A larger value of w_{ins} results in a lower flux leakage, lower unaligned inductance, and further needs a lower DC link voltage for the rated operation. However, the outer diameter increases more in this case which will increase the size of the motor. Therefore, the value of w_{ins} should be selected

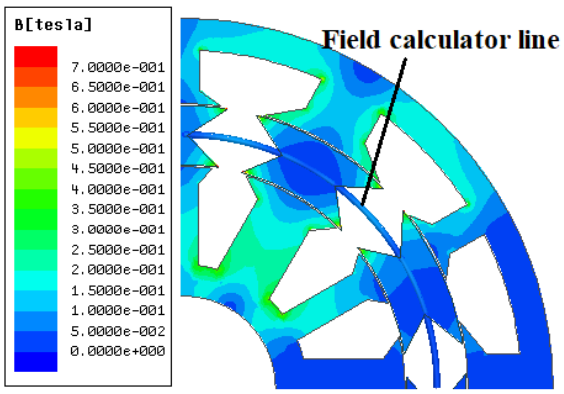

(a)

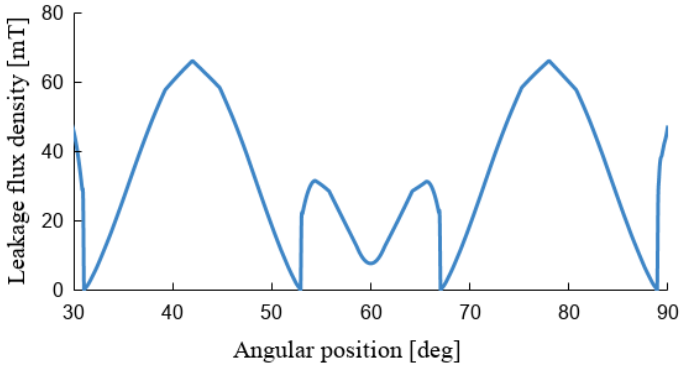

(b)

Figure 5.11: Calculation of leakage flux density in DSSRM1. (a) Flux density distribution at the unaligned position. (b) Leakage flux density calculated on the field calculator line in the middle of the rotor segments.

with a better compromise between the flux leakage and outer diameter of the machine. To calculate the value of w_{ins}, first, the flux density in the middle of rotor segments of DSSRM1 is calculated. Fig. 5.11 (a) shows the flux density plot in DSSRM1 at unaligned rotor position for half of the peak phase current. A field calculator line is drawn passing through the middle of the rotor segments to calculate the leakage flux density on it. Fig. 5.11 (b) shows the value of leakage flux density (B_{leak}) calculated on this line between 30° to 90° mechanical positions of the motor. It is observed that the maximum value of B_{leak} is 66 mT. With the insertion of the non-magnetic isolator between the half rotor segments, it is considered that the maximum value of B_{leak} should not be much more than 70 mT. The value of B_{leak} in the middle of the half rotor segments at the unaligned

position for the proposed DSSRM3 is given in Eq. (5.3)

$$B_{leak} = \frac{N_{slot}\ I_{ph}\ \mu_0}{2l_g + w_{ins}} \tag{5.3}$$

where I_{ph} is the phase current, N_{slot} is the conductors/slot, and l_g is the length of each air-gap. As per Eq. (5.3), the analytical value of w_{ins} for the considered leakage flux density of 70 mT is 13.5 mm. However, the value of leakage flux density, the outer diameter of the motor, and the % increase in outer diameter are calculated through FEM analysis for the variation of w_{ins} with a parametric step of 1 mm. Table 5.2 gives the results of this analysis. It is seen that the leakage flux density decreases with an increase in w_{ins}; however, the outer diameter of the motor increases. The value of w_{ins} for the considered leakage flux density of 70 mT will lie between 12 and 13 mm. Therefore, the calculation is further extended for the value of w_{ins} of 12.5 mm. The values of leakage flux density and outer diameter are 70.1 mT and 219 mm, respectively, which are acceptable. This value of w_{ins} is considered for the further study in this work.

Table 5.2: Comparative data for the variation of w_{ins}

Width of non-magnetic region (w_{ins})	12 mm	13 mm	14 mm
Leakage flux density (B_{leak}) in mT	72.9	67.7	63
Outer diameter of motor in mm	218	220	222
% increase in outer diameter	9	10	11

5.4.3 Modification in the Arc Angle of Outer Rotor Segments/Stator Poles

In the presented analysis, the design of a hypothetical DSSRM, as shown in Fig. 5.6, is presented which has a reduced torque ripple. Now the objective is to achieve nearly same torque characteristics in the proposed DSSRM as obtained in the hypothetical machine. In order to achieve this, the inductance profile of the proposed machine must match with that of the hypothetical machine. However, with the insertion of the non-magnetic region between half rotor segments, the arc lengths of the outer half rotor segments and stator poles increase for the same arc angle before the insertion. This will increases the flux linkage and inductance value of outer stator winding at all angular positions. The change

in the inductance profile will lead to the difference between desired and actual responses. Therefore, to achieve the desired response in the proposed motor, the optimization of the dimentions β'_r, β'_{exc} and β'_{aux} (as shown in Fig. 5.2) are investigated in such a way that the absolute error between the phase inductance of proposed and hypothetical machine should be minimum. Thus, the cost function for the given optimization problem can be obtained as

$$C = \min \left(\int \mid L_{DSSRM2} - L_{DSSRM3} \mid \right) \tag{5.4}$$

The cost value is calculated between 13° to 22° rotor position range. This range is considered because it is the effective torque generating region, better considers the excitation and demagnetization process, and better differentiates the variation of pole arc angles. The design variables used for optimization and their ranges of variation are given in Table 5.3.

Table 5.3: List of variables defined for optimization.

Variable	Range
β'_r	26°–30°
β'_{exc}	24°–28°
β'_{aux}	12°–16°

The discussed optimization problem can be easily solved on ANSYS Electromagnetics platform using optimetrics analysis. A 2-D model of the machine is prepared on the software, and the optimization setup is formulated in which the cost function given in Eq. (5.4) is defined using the setup calculation. The optimization condition is set to minimize. To perform this optimization analysis, Genetic Algorithm method is used. The optimized values of the various parameters obtained are given in Table 5.4.

The optimized dimensions are used in the proposed machine model for verification of the inductance profile. The FEM analysis of the Machine model with optimized dimensions is performed, and the analysis results of the inductance profile are found to match that of the hypothetical machine between 13° to 22° rotor positions as shown in Fig. 5.12. Therefore, these optimized values are considered to further analyze the dynamic response of the proposed machine.

Table 5.4: Optimized values of the parameters.

Variable	Optimized value
β'_r	27.84°
β'_{exc}	26.48°
β'_{aux}	14.12°

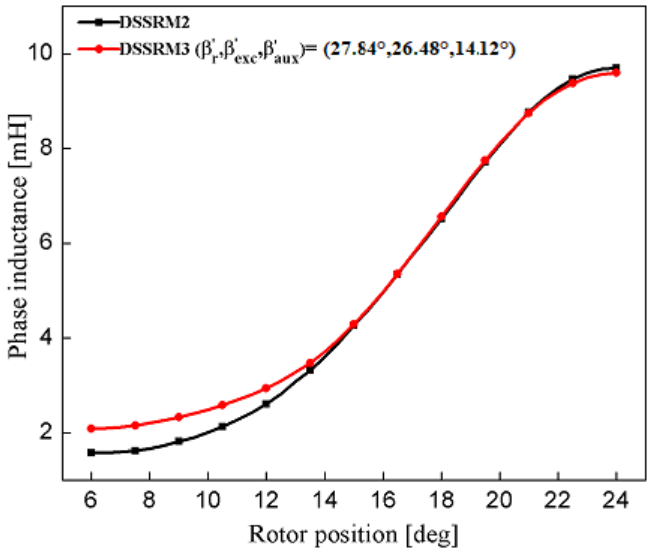

Figure 5.12: Matching of inductance profile of DSSRM2 and DSSRM3 between 13° to 22° rotor position.

5.5 Simulation Results

Table 5.1 deals with the design parameters of the DSSRM1. The modifications in the parameters for the proposed DSSRM3 are discussed in Section 5.4 and the modified parameter values are listed in Table 5.5. To simulate the performance of the proposed motor, 2-D FEM modelling is carried out, owing to its high accuracy for radial flux machines. The electromagnetic responses are achieved using ANSYS/MAXWELL software. The steps involved in the FEM study are modelling, material assignment, boundary assignment, meshing and excitation. 'steel-1008' available in the software library is used for the stator and rotor cores with 0.4 mm lamination width. An odd symmetry boundary is used for the creation of hypothetical boundary in DSSRM2. The driving circuits

Table 5.5: Modified parameter values for the proposed DSSRM.

Parameter	Value
Width of non-magnetic region w_{ins}	12.5 mm
Outer diameter of motor	219 mm
β'_r	27.84°
β'_{exc}	26.48°
β'_{aux}	14.12°

used to simulate the dynamic response of the DSSRM1 and DSSRM3 are asymmetric half-bridge converters which utilise two power switches per phase winding and provide maximum control flexibility. However, as per specific application by compromising with control flexibility, other known converters can also be utilised, which require less than two switches per phase winding [90]. Hysteresis current control with the bandwidth of ±0.5 A is considered to limit the phase current. The turn-on and turn-off angles for the phases are 0° and 14.3° (mech.), respectively.

Figures 5.13 (a) and 5.13 (b) show the static torque profiles for the inner and outer stators, respectively. It is shown that the outer stators torque is peakier than the inner stator for the same value of phase current. This will add some peaky response in the resultant output torque. Fig. 5.14 represents the flux density distribution in the proposed model at the rated operating condition and at 90 (elec.) and 150 (elec.) rotor positions, respectively. Fig. 5.15 shows the simulated steady-state response of DSSRM3 at rated speed. For high output torque and low torque ripple, the phase current overlapping technique is used in both cases. The output torque of the DSSRM1 has the values of T_{avg}, T_{pk2pk}, and % T_{ripple} as 33.6 N-m, 41.6 N-m, and 123.8%, respectively, which is shown in Fig. 5.3. It reveals the presence of a high torque ripple in the this motor. Fig. 5.15 represents the simulated response of DSSRM3 at the rated speed. In Fig. 5.15(a), i_a, i_b, and i_c are the phase currents of the inner stator windings whereas i'_a , i'_b, and i'_c are the phase currents of the outer stator windings. This figure shows that the motor is operating in SPC mode. Fig. 5.15 (b) shows the dynamic variation of output torque in

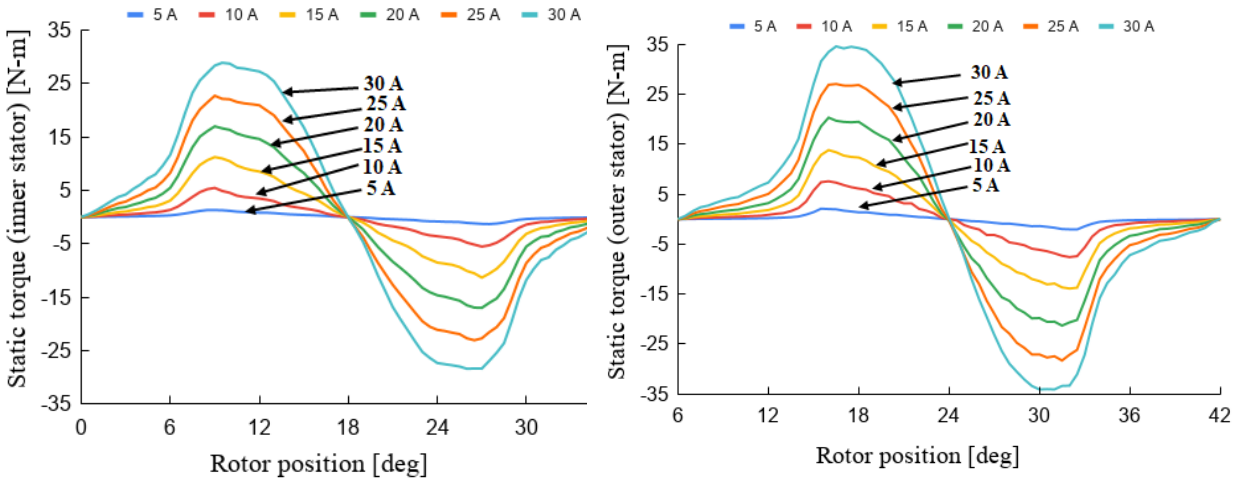

(a) (b)

Figure 5.13: Static torque profiles for inner and outer stator. (a) Static torque for inner stator. (b) Static torque for outer stator.

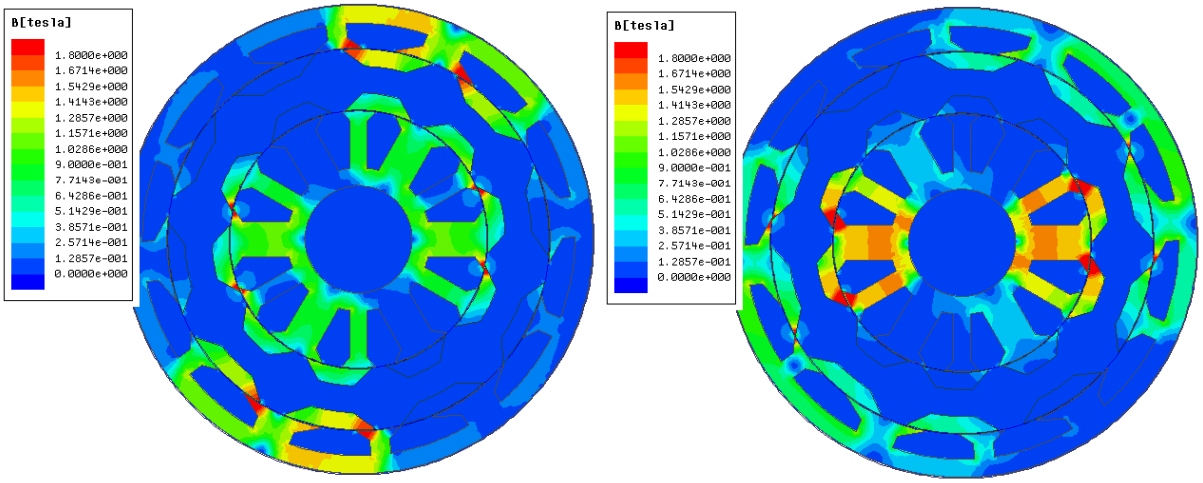

(a) (b)

Figure 5.14: Flux density distribution in the proposed model at 90 (elec.) and 150 (elec.) rotor position with respect to phase A and rated operating condition. (a) 90 (elec.) rotor position. (b) 150 (elec.) rotor position.

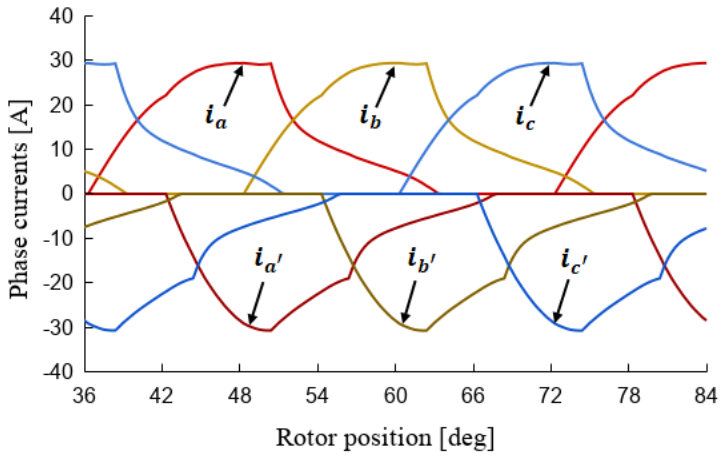

(a)

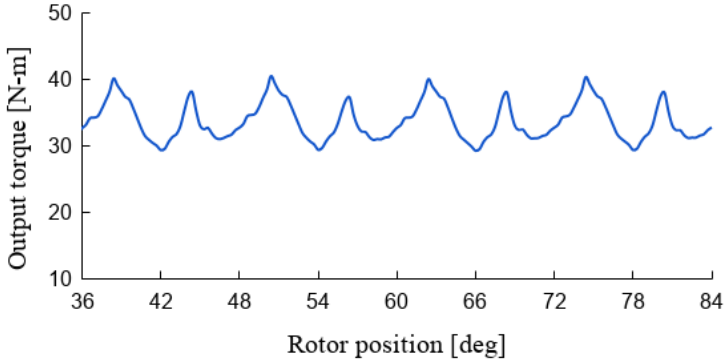

(b)

Figure 5.15: Steady-state response of DSSRM3 at rated speed of 1000 rpm. (a) Phase currents (b) Output torque.

the proposed motor. The values of T_{avg}, T_{pk2pk}, and % T_{ripple} are 33.7 N-m, 10.5 N-m, and 31.1%, respectively, in this case. It discloses that the torque ripple is significantly reduced in this case. Table 5.6 deals with the comparative data for DSSRM1 and DSSRM3 at the rated speed. The total loss through copper and core loss are 478 W and 479 W in the baseline and proposed DSSRM, respectively. The copper loss is lower in the proposed DSSRM than the baseline DSSRM because of the slight decrease in required per phase average and rms currents. However, the core loss is higher than that of the baseline DSSRM because of the increase in leakage flux. The efficiencies are comparable in both cases.

Figure 5.16 compares the dynamic torques of both motors at the rated speed. In the figure, it is seen that the peak-to-peak torque ripple is relatively low in the case of the proposed motor; subsequently, torque ripple is reduced by 74.9% compared to the

Table 5.6: Comparative data for DSSRM1 and DSSRM3 at rated speed.

Parameter	DSSRM1	DSSRM3
Rotor speed in rpm	1000	1000
Average torque (T_{avg}) in N-m	33.6	33.7
Peak to peak torque ripple (T_{pk2pk}) in N-m	41.6	10.5
Torque ripplr (T_{ripple}) in %	123.8	31.1
Core loss in W	93	109
Copper loss in W	385	370
Rated efficiency in %	88.0	88.0

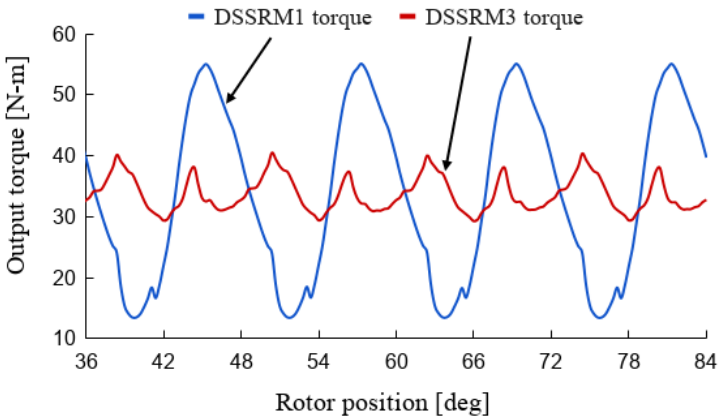

Figure 5.16: Comparison of the dynamic torques of DSSRM1 and DSSRM3 at the rated speed.

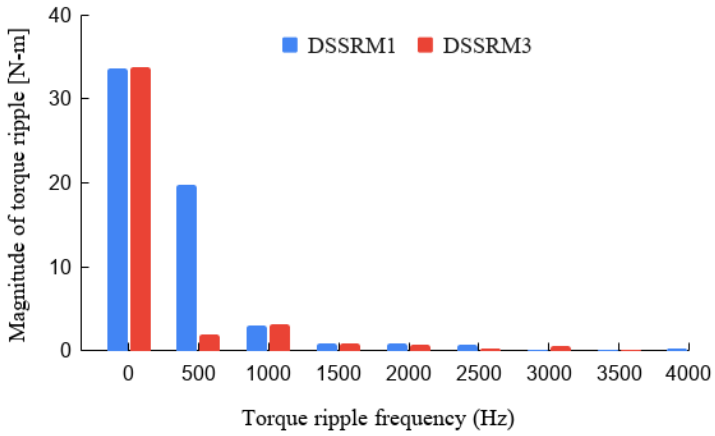

Figure 5.17: Comparison of torque ripple harmonics showing the reduction in lower order torque harmonics in proposed DSSRM.

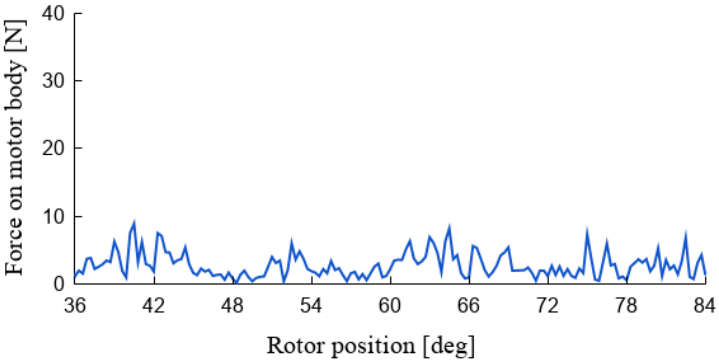

Figure 5.18: Resultant force working on the whole motor body of DSSRM3.

baseline motor. It is also seen that there are some peaky responses in the output torque of the proposed motor near 39°, 51°, 63°, and 75° rotor positions. This is because of the peaky static torque profiles of the outer stator, as seen in Fig. 5.13. Fig. 5.17 shows the harmonics analysis of torque ripple frequencies for both motors. The DC or average values of the torques are 33.6 N-m and 33.7 N-m for the baseline and proposed DSSRM, respectively. The fundamental and most dominant harmonics is 500 Hz. The magnitude of this harmonics for baseline and proposed DSSRM are 59.0% and 6.0% of the DC value, respectively. Therefore, this harmonic is reduced by 53.0% in the proposed motor. It prevails that low-frequency torque ripple is reduced in the case of the proposed motor. Fig. 5.18 shows the resultant force working on the whole motor body of the proposed DSSRM at rated condition. The average value of this force is 3.6 N which is ignorable.

In the case of the baseline DSSRM, this value is 2.0 N.

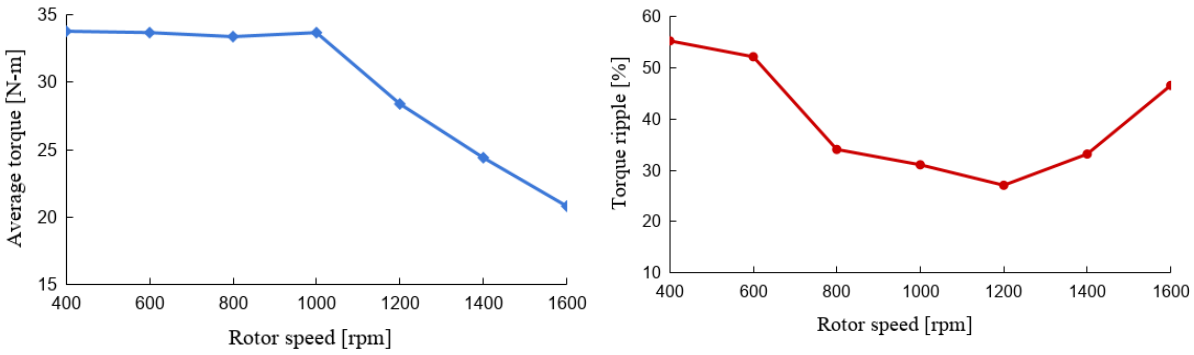

(a) (b)

Figure 5.19: Output torque and torque ripple of proposed DSSRM with rotor speed. (a) Output torque. (b) Torque ripple.

Figure 5.19 (a) represents the output torque of the proposed motor with the variation of rotor speed. Below the base speed, the output torque is maintained constant by maintaining the average value of the phase current nearly constant through the hysteresis current control method. In SRMs, output power decreases above the base speed. This is because, with the increase in rotor speed, the back EMF increases, and the time provided to increase the phase current also decreases. This reduces the phase current and subsequently reduces the output power above the base speed. Phase current advancing technique is employed to maintain the output power above the base speed [95]. In this technique, phases are energized before the actual turn-on position. It increases the phase current and maintains the constant output power above the base speed. Fig. 5.19 (b) shows the torque ripples with the variation of the rotor speed. It shows that comparatively lower torque ripples occur near the rated speed between 800 and 1400 rpm. This is because, in this speed range, the falling torque region of one stator is better compensated by the rising torque region of the other one and vice-versa. The minimum value of torque ripple is 27.1% which occurs at 1200 rpm rotor speed. The above observations envisage that such a motor can be employed in applications where a lower torque ripple is required at a higher operating speed.

5.6 Conclusions

A new DSSRM has been proposed in this chapter which has significantly low torque ripple at higher operating speed. Firstly, a hypothetical DSSRM has been discussed, which has a very low torque ripple. Thereafter, some modifications and compromises have been added to the proposed motor to achieved nearly same torque characteristics as in the hypothetical motor. In the proposed motor, the outer stator is shifted by half of the stroke angle with respect to the inner stator. The phase windings of the inner and outer stator are excited parallelly with the same phase shift. Each rotor segment is divided into two halves, and a wide non-magnetic isolator is inserted between them. Modifications are done in outer stator poles and outer half rotor segments, after this insertion. It is observed in the simulation results that the proposed motor has significantly reduced torque ripple near the rated speed.

The next chapter summarizes the work in the thesis, points out the contributions and limitations and also forecasts some possible endeavours in the context of DSSRM design.